INORGANIC CHEMISTRY FRONTIERS

RESEARCH ARTICLE

View Article Online
View Journal

Cite this: DOI: 10.1039/d6qi00081a

Electrochemical ammonia synthesis from a bis-aryloxy-carbene-molybdenum nitride complex

Théo Personeni,†[a,b] Xueli Wang,†[a] Julien Babinot,[a] Soussana Azar,[c] Malo Duquesnoy,[b] Stéphane Bellemin-Laponnaz,[c] Lhoussain Krhouz,[b] Nathalie Saffon-Merceron,[d] Marie Fustier-Boutignon,[a] Eric Clot,[e] Christophe Bucher *[b] and Nicolas Mézailles *[a]

The electrocatalytic reduction of dinitrogen to ammonia by molecular complexes is fundamentally limited by poorly understood proton–electron transfer sequences and catalyst deactivation pathways. Here we report a detailed mechanistic investigation of nitrogen reduction mediated by a Mo(VI) nitride complex involving a bis-aryloxy-carbene ligand. Combined electrochemical, spectroscopic, and computational studies reveal stepwise electron transfer and proton transfer processes proceeding through Mo(V) imide and Mo(IV) amide intermediates. Notably, we demonstrate that a Mo(V) imide intermediate undergoes a key disproportionation reaction producing the corresponding amide species, ultimately enabling NH_3 formation. We also establish that the catalytic activity is impeded by competitive chloride coordination and the formation of a stable Mo(III) dimer that prevents N_2 binding. These findings identify critical mechanistic bottlenecks in molecular N_2 electroreduction and establish clear ligand-design criteria for suppressing deactivation pathways and enabling efficient ammonia synthesis under mild conditions.

Received 17th January 2026,
Accepted 14th April 2026

DOI: 10.1039/d6qi00081a

rsc.li/frontiers-inorganic

Introduction

The N_2 to NH_3 reduction involves a challenging 6 electrons–6 protons transfer and is currently achieved in industry *via* the Haber–Bosch process requiring drastic conditions, thus leading to massive CO_2 emission.[1–4] The discovery in the mid-sixties of the first coordination complex $[Ru(NH_3)(N_2)]^{2+}$ incorporating nitrogen as a ligand opened up the possibility to develop milder approaches, *i.e.* using homogeneous chemistry, to activate and functionalize N_2.[5–8] Since then, numerous studies have shown that the activation mechanism depends both on the nature of the metal center and on the ligand platform, and that a rational development of efficient catalysts requires understanding the elementary steps involved in the activation of N_2 at the metal center.[2,3,8–16] However, few of them focus on the electrocatalytical nitrogen reaction reduction using coordination complexes, and even fewer on mechanistic studies.[11–14,17–20] In this article, we present a new electrochemical ammonia synthesis reaction using a bis-aryloxycarbene-molybdenum nitride complex. Based on extensive electrochemical, spectroscopical characterization and theoretical calculations, intermediates have been identified and a reaction mechanism is proposed.

Among the metal complexes used so far in this context, those based on Mo have been the most studied and are today by far the most effective. In particular, Schrock designed tunable tris-amido-amine ligands $(N_3N)^{3-}$ forming C_{3v} symmetry complexes with Mo that led to the discovery of the first N_2-to-NH_3 catalytic process 20 years ago (Scheme 1A).[9] In a series of papers, they studied the protonation and electron transfer steps and isolated several key intermediates involved in the proposed catalytic cycle.[16,22] Most notably, the ligand was designed to favor the formation of an end-on Mo–N≡N complex, while preventing the formation of the corresponding Mo–N≡N–Mo dimer which hamper functionalization at the N centers. They brought to light the sequential functionalization of the nitrogen atoms with one electron and one proton and isolated the stable nitride complex $(N_3N)Mo(VI)\equiv N$ after addition of three protons/three electrons to the dinitrogen complex $(N_3N)Mo(III)(N_2)$. The authors also established that the N center of the nitride function is a rather weak base that can be fully protonated with a strong acid such as $[H(OEt_2)_2][BAr'_4]$ and only partially (25%) with a weaker acid such as [2,6-LutH][BAr'_4]. The cycle was subsequently computed by Tuczek,

[a]Université de Toulouse, CNRS, LHFA – UMR 5069, 118 route de Narbonne, 31062 Toulouse Cedex, France. E-mail: nicolas.mezailles1@univ-tlse3.fr
[b]CNRS, ENS de Lyon, LCH, UMR 5182, 69342 Lyon cedex 07, France
[c]CNRS-Université de Strasbourg, Institut de Physique et Chimie de Strasbourg, UMR7504, 23 rue du Loess—BP43, 67034 Strasbourg Cedex 2, France
[d]Université de Toulouse, CNRS, ICT – UAR2599, 118 route de Narbonne, 31062 Toulouse, France
[e]ICGM, Univ. Montpellier, CNRS, ENSCM, Montpellier, France
†Contributed equally.

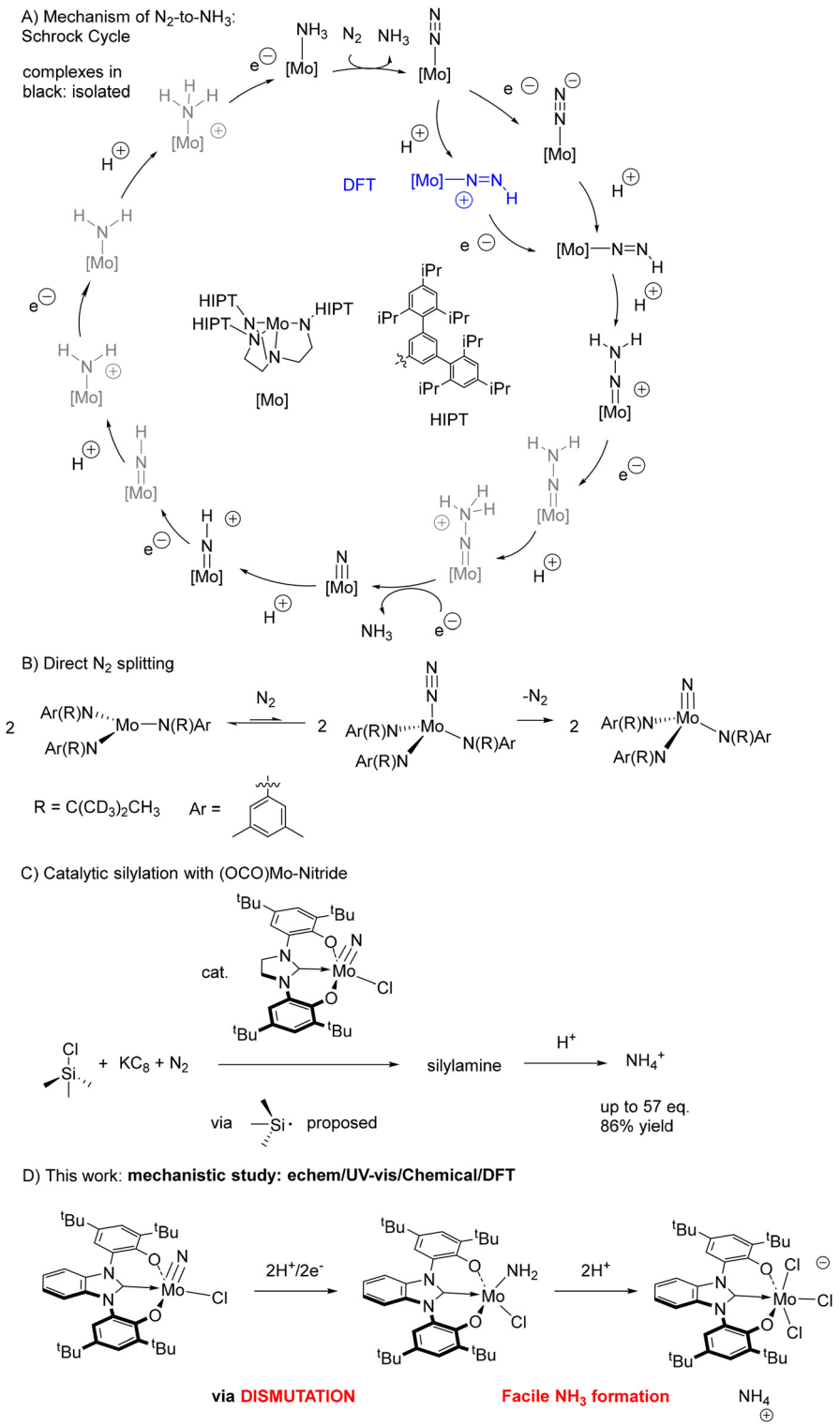

Scheme 1 Context of the present study (D) put into perspective with regard to the work of (A) Schrock,[9] (B) Cummins,[10] and (C) Hu.[21]

who confirmed the "strictly" alternating "one proton/one electron" sequence of events.[23] They pointed a very strong driving force for N–N splitting from the $(N_3N)Mo(N–NH_3)^+$ intermediate leading to the first equivalent of NH_3 and $(N_3N)Mo(N)$.

On the other hand, Cummins reported in 1995 the first example of a direct N_2 cleavage (Scheme 1B). A designed trisamido complex, $Mo(NRR')_3$ Mo(III) is capable of N_2 coordination to yield the $(NRR')_3Mo–N{\equiv}N–Mo(NRR')_3$ μ-end-on dimer. This

intermediate allows a six electron transfer (3 per Mo center) to the σ* and π* orbitals of the N_2, yielding the nitride complex $(NRR')_3Mo(N)$ Mo(VI).[10] Subsequent NH bond formation was not reported with this complex which appears to require quite strong electrophiles to functionalize the terminal nitrogen atom, such as acyl triflates.[24] One of the main drawbacks of using amide ligands with Mo complexes is their strong basic character which can affect the protonation equilibria involved in the medium and lead to a deactivation/decomposition of the catalyst. Several groups have built on these results, demonstrating facile N_2 splitting with group 6 and 7 metal complexes. Nishibayashi, Yoshizawa and coworkers have reported in the past years impressive catalytic results in N_2-to-NH_3 transformation, relying on both N_2 splitting and proton coupled electron transfer (PCET), using SmI_2/ROH, including H_2O, as electron/proton source respectively.[25,26] Recent efforts by Peters have been directed to transpose this PCET chemical process into an electrochemical one, that would avoid the generation of stoichiometric Sm(III) waste (three equivalents per equivalent of NH_3 produced).[17] It should be noted that, despite their undeniable interest, the performance of the electrochemical approaches remains significantly inferior to that of the chemical ones. This calls for massive research in the electrocatalytic nitrogen reduction into ammonia.

While this work was underway, Hu reported the catalytic silylation of N_2 using a (OCO)MoNCl complex featuring a related bis-aryloxy-carbene ligand (with a saturated carbene moiety, see Scheme 1C). Most importantly, they demonstrated the highest yield (86%) and good TON (57) for this transformation, and proposed silyl radical functionalization of N_2. The (OCO)MoNCl platform is therefore of interest for the studies of N_2 fixation.[21]

In this work, we endeavored the electrocatalytic N_2-to-NH_3 synthesis using a Mo≡N complex incorporating a bis-aryloxy-carbene ligand previously designed by some of us.[27–31] We present a full investigation of the stepwise H^+/e^- addition events using a coupled electrochemical/UV-visible/ESR approach. We highlight here an unprecedented mechanism leading to the amide [(OCO)Mo(NH_2)Cl] complex involving dismutation of the imide [(OCO)Mo(=NH)Cl] complex. Chemical syntheses of the intermediates in the N-functionalization steps revealed easy reduction of the Mo(VI) nitride complex, facile NH_3 formation and dissociation from the Mo(IV) center. Finally, DFT calculations not only fully rationalize these experimental findings, but also provide key insights into the possible bottlenecks of the N_2 functionalization using this ligand framework.

Results and discussion

Synthesis and characterization of the nitride complexes [(OCO)Mo(≡N)Cl] ([1^{VI}]) and [(OCO)Mo(≡N)Cl]$^-$ ([Cp_2Co]$^+$ [1^V]$^-$ [Cp_2Co]$^+$)

Complex [1^{VI}] was synthesized in a one-step procedure involving an acid–base reaction between the ligand [H_3L]Cl and the metallic nitride precursor [(O^tBu)$_3$Mo(N)] (Scheme 2).[30,32,33] After 48 hours of stirring at room temperature and concentration of the reaction mixture, the addition of *n*-pentane yielded a purple precipitate of complex [1^{VI}] which was isolated in 73% yield. The ^{1}H NMR spectrum recorded for this diamagnetic Mo(VI) complex [1^{VI}], is in agreement with the proposed structure incorporating a central carbene unit (Fig. S22–S27). It is worth mentioning that this synthesis was independently reported by Hohloch *et al.* during the writing of this manuscript.[34] Note that all attempts to form complex [1^{VI}] by reaction of the deprotonated ligand L^{3-} ("O–C–O") with [Mo(N)Cl_3]$_4$ failed.

Single crystals suitable for X-ray diffraction were obtained by layering a solution of [1^{VI}] in dichloromethane with pentane (Fig. 1). The obtained structure presented in Fig. 1 reveals that the first coordination sphere of the Mo center forms a distorted pyramid with a square base, which is identical to that described by Hohloch *et al.* The two oxygen atoms are located opposite to each other, and the nitrogen atom is at the tip of the pyramid. The length of the Mo≡N measured at 1.649(1) Å is within the typical range of a Mo(VI) nitrido bond.[35,36] The Mo–C length of 2.205(1) Å is also characteristic of metal–carbene bonds.[37,38]

Electrocatalytic properties of complex [1^{VI}] in presence of a proton source

The ability of complex [1^{VI}] to promote the reduction of nitrogen in the presence of protons was assessed under catalytic conditions using acetonitrile tetra-*n*-butylammonium bis-trifluoromethanesulfonimidate (TBATFSI) as an electrolyte. Lutidinium triflate (LutHOTf) was selected as the proton source for (electro)catalytical experiments considering the poor solubility of the corresponding halide derivatives in the

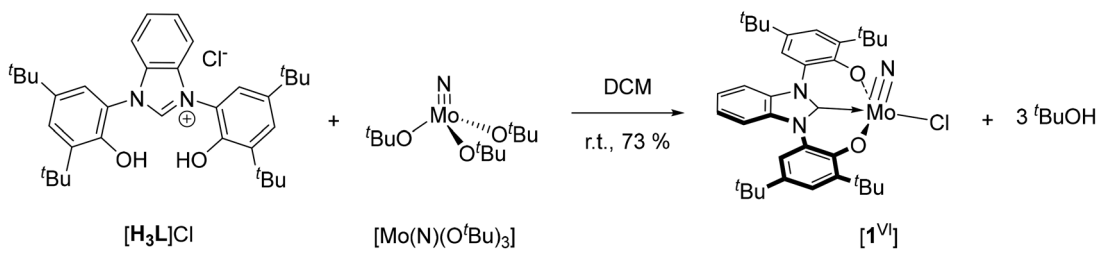

[H_3L]Cl [Mo(N)(O^tBu)$_3$] [1^{VI}]

Scheme 2 Synthesis of complex [1^{VI}].

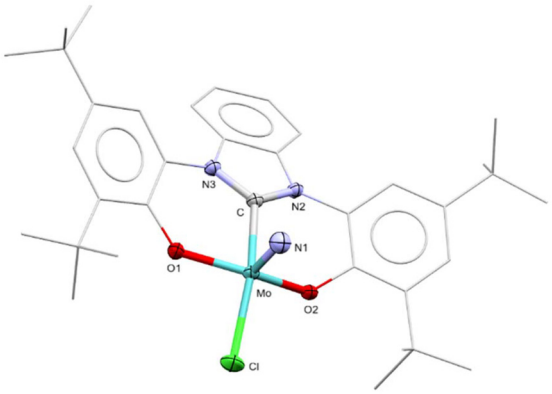

Fig. 1 Molecular structure of [$\mathbf{1}^{VI}$] obtained by single crystal X-ray diffraction. Hydrogen atoms are omitted for clarity. Ellipsoids are drawn for a 50% probability.

electrolyte. The cyclic voltammogram recorded in the presence of an excess of LutHOTf is shown in SI (Fig. S12). It demonstrates that the hydrogen evolving reaction (HER) occurs at −1.7 V (*vs.* Ag^+ (10^{-2} M)/Ag). Controlled potential electrolyzes were thus conducted at more positive potential values to prevent the unwanted HER, at room temperature in a dedicated glovebox operating under N_2 using a homemade divided cell and a glassy carbon foam working electrode. After electrolysis, the samples were subjected to hydrolysis (excess HCl) and the quantity of NH_4^+ formed was quantified by NMR spectroscopy measurements using a calibration curve (see SI, Fig. S1). The results obtained by varying the applied potential, the dissolved gas and the electrolyte are presented in Table 1. These data reveal that the amount of ammonia obtained is not catalytic but only super-stoichiometric (Table 1, entries 1 and 2). Measurements carried out under argon (entry 3) produced one equivalent of ammonium chloride, which demonstrated the stoichiometric functionalization of the starting molybdenum nitride complex [$\mathbf{1}^{VI}$] by an excess of acid/electrons. Inspired by previous work showing the positive effect of iodide anions on the nitrogen splitting reaction involving molybdenum complexes,[39] the same electrolysis was conducted by replacing TBATFSI with tetra-*n*-butylammonium iodide (TBAI). The data shown in entry 4 reveal that this change has no significant effect on the outcome of the reaction (Table 1, entry 4). Overall, the results of entries 1, 2 and 4 (under N_2) *vs.* 3 (under Ar) demonstrated that the species formed after functionalization of the N center of the nitride does not allow the subsequent functionalization of N_2.

Additional experiments were also carried out to evaluate the properties of complex [$\mathbf{1}^{VI}$] under chemical catalysis conditions, using Cp_2Co as a reducing agent and $LutH^+$ as a proton source. The amount of ammonia formed under these conditions was also found to be low (TON ≈ 1, yield ≈ 1.7%), which indicates that the system does not function catalytically under either chemical or electrochemical conditions.

We therefore studied in detail the reactivity of complex [$\mathbf{1}^{VI}$] in order to understand the N-functionalization sequence by protons and electrons and to identify the blocking points that prevent the existence of a catalytic process.

As mentioned above, it is now well known that high oxidation state metal-nitrides of group 6 metals exhibit very weak nucleophilic and basic properties. These features can be rationalized by the strong donation of the formal N^{3-} ligand toward the metal center. In accordance with this, we first established on the ground of ^{1}H NMR and UV-visible absorption spectroscopy measurements (Fig. S17) that the nitride ligand in [$\mathbf{1}^{VI}$] is not basic enough to react with protons, even when added in excess lutidinium chloride (LutHCl).

Complex [$\mathbf{1}^{VI}$] was then subjected to cyclic voltammetry (CV) and UV-visible absorption spectroscopy measurements carried out in acetonitrile in presence of TBATFSI. In agreement with the preliminary data reported by Hohloch *et al.*[34] the CV curves display a Nernstian one electron reduction wave at $E_{1/2}$ = −0.69 V and three successive irreversible reduction waves at E_p = −2.10, −2.68 and −2.94 V (Fig. 2). The first reduction wave, attributed to the one-electron reduction of the Mo^{VI} center, was found to be reversible at all scan rates investigated (5 and 1000 mV s^{-1}, see Fig. S2). The following fully irreversible reduction waves observed below −2 V were attributed to subsequent reductions of the Mo^V coupled to chemical processes. The diffusion coefficient of [$\mathbf{1}^{VI}$] was estimated at 1.32 × 10^{-5} cm^2 s^{-1} from the Cottrel equation (Fig. S3) and the number of electrons involved in the first reduction wave was estimated to be 1 by exhaustive controlled potential electrolysis (see below). The UV-visible absorption spectrum of [$\mathbf{1}^{VI}$]

Table 1 Results of electrolysis experiments carried out in potentiostatic regime with millimolar (1 mM, 5 mL) solutions of [$\mathbf{1}^{VI}$] in acetonitrile + TBA·TFSI/TBA·I (0.1 M), followed by hydrolysis of the crude mixture with an excess of HCl. E_{app} (volts *vs.* $AgNO_3$ (10^{-2} M)/Ag) is the potential applied at a glassy carbon foam working electrode. The yield, FE and TON values were calculated by averaging **2** experiments (standard variation given). TON is defined as the amount of NH_4^+ per amount of complex, yield = $4n(NH_4^+)/n$(LutH·OTf); FE = $3n(NH_4^+)F/Q$, where $n(NH_4^+)$ and n(LutH·OTf) are the number of moles of ammonium and lutidinium triflate, respectively. F is the Faraday constant and Q the charge (in Coulomb) consumed during electrolyses

Ent.	Electrolyte	$LutH^+OTf^-$: [$\mathbf{1}^{VI}$]	E_{app} (V)	Charge (C)	Yield (%)	FE (%)	TON
1[a]	TBATFSI (0.1 M)	50 : 1	−1.4 V	−7 C	11.2 ± 0.6	28.9 ± 0.7	1.4 ± 0.1
2[a]	TBATFSI (0.1 M)	50 : 1	−1.6 V	−7 C	12.6 ± 0.7	32.3 ± 1.7	1.6 ± 0.1
3[b]	TBATFSI (0.1 M)	50 : 1	−1.6 V	−7 C	8.4 ± 0.5	21.8 ± 1.2	1.0 ± 0.1
4[a]	TBAI (0.1 M)	50 : 1	−1.4 V	−7 C	12.6 ± 0.7	32.3 ± 1.7	1.6 ± 0.1

[a] Controlled potential electrolysis performed under N_2. [b] Controlled potential electrolysis performed under Ar.

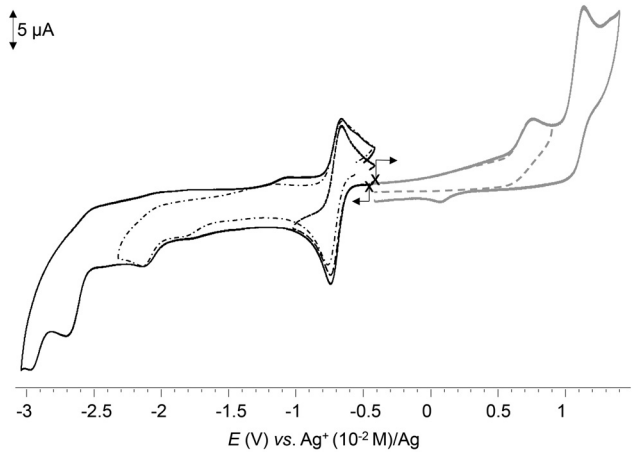

Fig. 2 Cyclic voltammetry (CV) curves recorded for a 1 mM solution of [$\mathbf{1}^{VI}$] in acetonitrile + TBATFSI (0.1 M) (WE: GC (∅: 3 mm), ref: $Ag^{+}(10^{-2}$ M)/Ag, ν = 100 mV s^{-1}).

(Fig. 3B) displays two main absorption bands centered at λ_{max} = 302 nm (ε = 8797 L mol^{-1} cm^{-1}) and at λ_{max} = 500 nm (ε = 340 L mol^{-1} cm^{-1}), both attributed to ligand-to-metal charge transfer processes (Fig. S16).

These conclusion were further confirmed by exhaustive electrolysis experiments first revealing that the anionic complex [$\mathbf{1}^{V}$]$^{-}$, generated *in situ* by controlled potential electrolysis (CPE) at −1.0 V *vs.* Ag^{+}/Ag on platinum (Fig. 3A and B), is stable at the electrolysis time scale (hour) (Fig. 3A, inset). The advancement of the reduction was followed by UV-visible absorption measurement and the stability of the electrogenerated complex [$\mathbf{1}^{V}$]$^{-}$ was demonstrated with CV and rotating disk measurements carried out after addition of 1 e^{-} per moles. The accumulation of [$\mathbf{1}^{V}$]$^{-}$ results in the decrease of the absorption band at 302 nm and 500 nm and the appearance of an absorption band at 350 nm. ESR data collected at 110 K before and after reduction also confirmed the localization of the electron transfer on the metal center (Fig. 3B, inset). The silent ESR spectrum obtained with complex [$\mathbf{1}^{VI}$] (Fig. S19) evolved into an intense ESR signal which was assigned to a $S = \frac{1}{2}$ square-pyramidal Mo^{V} complex (Fig. S20, g_{av} = 1.958).[40–42] This analysis demonstrates the absence of ligand (*i.e.* solvent) on the Mo^{V} center in the trans position to the nitride ligand.

The electrochemical stability of the one electron reduction complex of [$\mathbf{1}^{VI}$] was finally validated by performing a chemical reduction of [$\mathbf{1}^{VI}$] in THF, using Cobaltocene (E° = −1.33 V *vs.* $Fc^{+/0}$) as a suitable one electron reducing agent.[43] Mixing [$\mathbf{1}^{VI}$] with cobaltocene in stoichiometric amount resulted in the formation of a grey precipitate of complex [$\mathbf{1}^{V}$]$^{-}$·Cp_2Co^{+}. X-ray diffraction analyses performed on single crystals obtained after a few days of slow evaporation of a saturated solution confirmed the structure. As can be seen in Fig. 4, the first coordination sphere around the Mo^{V} center exhibits a distorted square base pyramid geometry involving two oxygen, one carbon, one chloride and one nitrogen. The apical atom is the strongest trans effect ligand, N. This structure is consistent with the experimental data discussed above (CV, UV-visible absorption and ESR). An important feature of this complex is that the Cl^{-} ligand remains bound to the Mo^{V} center to form the zwitterionic complex [$\mathbf{1}^{V}$]$^{-}$·Cp_2Co^{+}. It is likely that the geometrical constraints brought by the OCO ligand (meridional coordination) precludes the formation of the tetracoordinated neutral [(OCO)MoN] complex, *via* Cl^{-} elimination, thereby corroborating the reversibility of the redox wave observed for complex [$\mathbf{1}^{VI}$]. The Mo≡N bond length is slightly shorter in [$\mathbf{1}^{V}$]$^{-}$ (1.627(7) Å) than in [$\mathbf{1}^{VI}$] (1.649(1) Å). A similar shortening

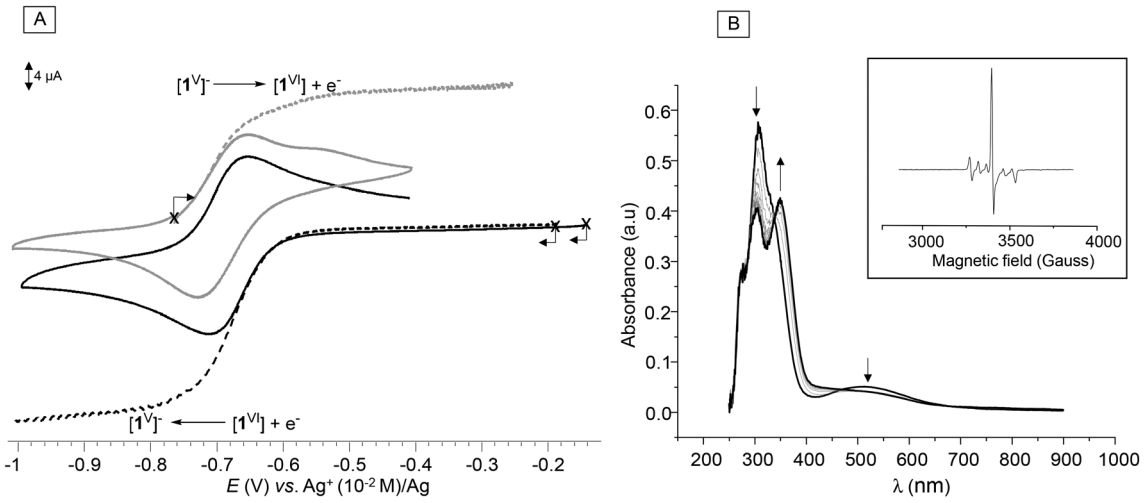

Fig. 3 (A) CV and RDV curves recorded for a solution of [$\mathbf{1}^{VI}$] (1 mM) in acetonitrile + TBATFSI (0.1 M) before (solid and dotted black lines) and after CPE at −1.0 V (grey and dotted grey, 1 electron per mole). (B) UV-visible absorption spectra (l = 1 mm) recorded during the CPE of [$\mathbf{1}^{VI}$] (1 mM) in acetonitrile + TBATFSI (0.1 M) at −1.0 V (1 electron per mole). Inset: ESR spectrum (X band) recorded at 110 K after CPE at −1.0 V. CV and RDE measurements were carried out on GC (∅: 3 mm, RDE: 3 mm), reference: $Ag^{+}(10^{-2}$ M)/Ag, *v*: 100 mV s^{-1} for CV and 20 mV s^{-1} for RDV (500 rpm), counter electrode: Pt wire/carbon in acetonitrile + TBATFSI. Electrolyses were carried out on platinum at E_{app} = −1 V.

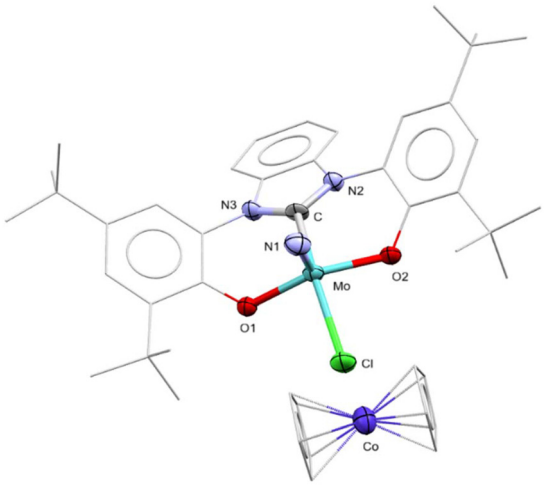

Fig. 4 X-ray structure of $[\mathbf{1}^{V}]^{-}$ Cp_2Co^{+}. Hydrogen atoms are omitted for clarity. Ellipsoids are drawn for a 50% probability.

of the Mo–C bond is observed upon reduction (Mo–C 2.156(7) Å in $[\mathbf{1}^{V}]^{-}$ *vs.* 2.205(1) Å in $[\mathbf{1}^{VI}]$), indicating a stronger interaction. On the other hand, the Mo–Cl bond is *ca.* 0.1 Å longer in $[\mathbf{1}^{V}]^{-}$ (2.447(2) Å) than in $[\mathbf{1}^{VI}]$ (2.349(3) Å). The increase of the Mo–Cl distance upon reduction could be explained by the presence of the single electron in an antibonding orbital of the Mo–Cl bond.

Mechanistic study of the reduction of $[\mathbf{1}^{VI}]$ in the presence of protons

Having demonstrated the stability of the reduced species $[\mathbf{1}^{V}]^{-}$, we expected that the increase in electron density would facilitate protonation. This hypothesis was readily verified by showing that the electrochemical signature of complex $[\mathbf{1}^{VI}]$ evolves significantly upon addition of acids. As can be seen in Fig. 5A, the first wave at $E_{1/2}$ = −0.69 V attributed to the one electron reduction of $[\mathbf{1}^{VI}]$ (Fig. 5A, black curve) loses its reversibility upon addition of LutHCl (pK_a = 6.7, Fig. 5A).[44] This result thus clearly demonstrates that the electrogenerated complex $[\mathbf{1}^{V}]^{-}$ is rapidly transformed into the monoprotonated complex $[\mathbf{2}^{V}]$ (OCO)Mo(=NH)Cl at the electrode. A detailed analysis of this evolution shows that the peak potential measured on the first reduction wave in the presence of 50 molar equivalents of LutHCl (Fig. 5A, dotted grey curves) varies linearly with the decimal logarithm of scan rate (50 to 5000 mV s^{-1}) with a slope of −27.7 ± 3.6 mV (Fig. 5B). Other studies revealed that this same peak potential value is independent of the concentration in complex $[\mathbf{1}^{VI}]$ (Fig. 5C) and that the intensity of the cathodic peak current, as well as the number of electrons exchanged, increases with the concentration of LutHCl. These results thus led us to consider either an ECE or an EC-disproportionation mechanism.[45] Further efforts were paid to discriminate between these two mechanisms.

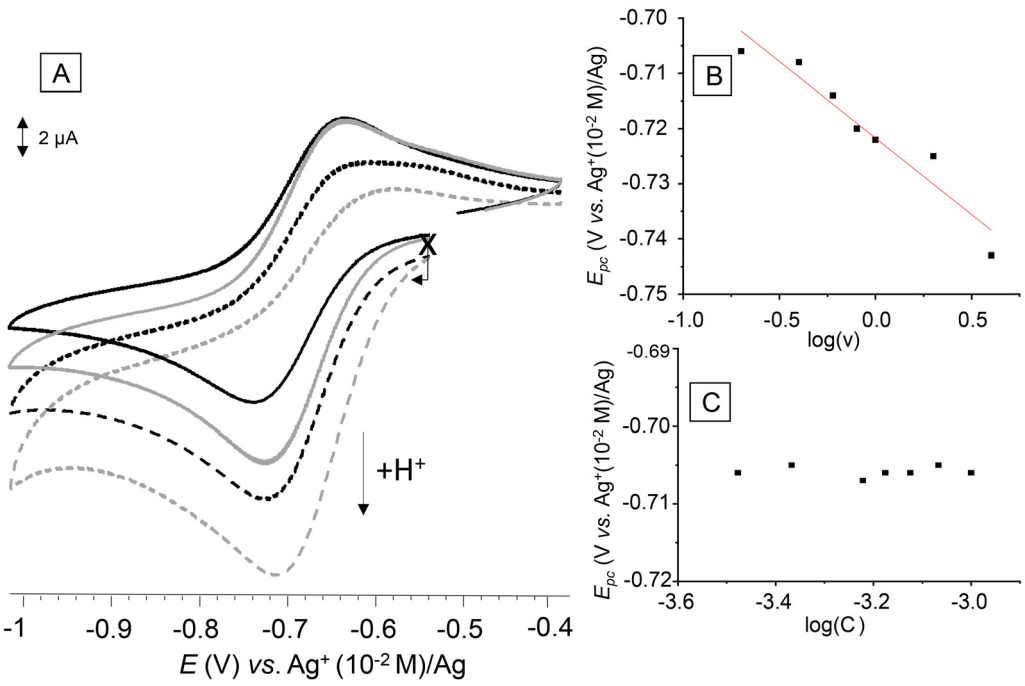

Fig. 5 (A) Cyclic voltammetry curves recorded for a solution of $[\mathbf{1}^{VI}]$ (1 mM in acetonitrile + 0.1 M TBATFSI) after addition of 0 (black), 1 (grey), 5 (dotted black) and 50 molar equivalents (dotted grey line) of LutHCl. (B) Evolution of the peak potential value as a function of scan rate (black square). The linear fit to the experimental data is shown in solid red line. (C) Evolution of the peak potential value measured for a solution of $[\mathbf{1}^{VI}]$ (1 mM in acetonitrile + 0.1 M TBATFSI) + 50 molar equivalent of LutH·Cl as a function of the concentration in $[\mathbf{1}^{VI}]$ (black square). WE: GC (∅: 3 mm), ref: $Ag^{+}(10^{-2}M)/Ag$, CE: Pt wire.

The first evidence was obtained by following the protonation of the electrogenerated anion $[\mathbf{1}^{V}]^{-}$ (obtained by CPE of a millimolar solution of $[\mathbf{1}^{VI}]$) by UV-visible absorption spectroscopy measurements. The spectra presented in Fig. 6A and B, recorded after addition of 1 molar equivalent of LutHCl, show a rapid development (t < 60 s) of an absorption band at 435 nm attributed to the protonated complex $[\mathbf{2}^{V}]$ [(OCO)Mo(=NH)Cl] (Scheme 2). In a second step, we then see that this band loses around 33% of its initial intensity in 1 h, while undergoing a blue shift up to 440 nm. The isosbestic point observed at 552 nm indicates that the protonated complex $[\mathbf{2}^{V}]$ undergoes a slow transformation, with an invariant stoichiometry over time. The kinetics of both successive steps could be estimated from those UV-visible data using second order kinetic models to k_1 = 175.2 L mol^{-1} s^{-1} and k_2 = 0.205 L^{-1} mol^{-1} s^{-1} (Fig. S18).

These reactions were also studied by electrochemical methods. The CV curves recorded 1h30 after the addition of 1 molar equivalent of LutHCl to a solution of the previously electrogenerated complex $[\mathbf{1}^{V}]^{-}$ show a reversible wave at $E_{1/2}$ = −0.69 V, attributed to the reduction of $[\mathbf{1}^{VI}]$, followed by a second irreversible reduction wave at E_p = −1.09 V (Fig. 7A, grey curve). The data recorded at a rotating electrode before and after one electron reduction of $[\mathbf{1}^{VI}]$ and addition of 1 molar equivalent of LutHCl also revealed that the diffusion limited currents measured on the two consecutive plateau at $E_{1/2}$ = −0.69 V and at E_p = −1.09 V are of the same intensity, each corresponding to half the initial reduction wave recorded with the starting solution of $[\mathbf{1}^{VI}]$ (Fig. 7B, grey and black curves).

The spectroscopic and electrochemical data discussed above, including the formation of $\frac{1}{2}$ equivalent of $[\mathbf{1}^{VI}]$ by protonation of $[\mathbf{1}^{V}]^{-}$, are thus consistent with the EC-disproportionation mechanism presented in Scheme 3. The first step is the one electron reduction of $[\mathbf{1}^{VI}]$ generating the basic anion $[\mathbf{1}^{V}]^{-}$ which undergoes a rapid protonation (within 1 minute) with

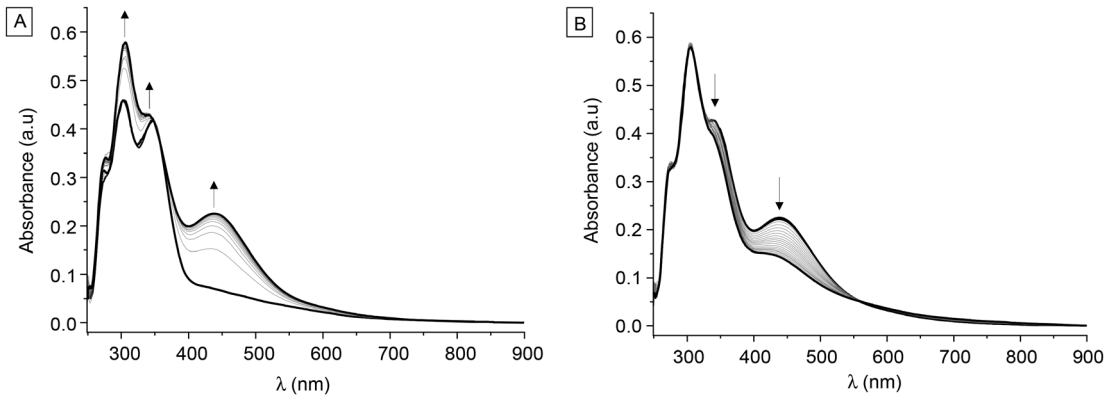

Fig. 6 (A) UV-visible absorption spectra recorded for $[\mathbf{1}^{VI}]^{-}$ (1 mM) + 1 molar equivalent of LutHCl: t0 to t0 + 1 min. (B) UV-visible absorption spectra of $[\mathbf{1}^{V}]^{-}$ (1 mM) + 1 molar equivalent of LutHCl t0 + 1 min to t0 + 60 min (acetonitrile + TBATFSI 0.1 M, optical path: 1 mm).

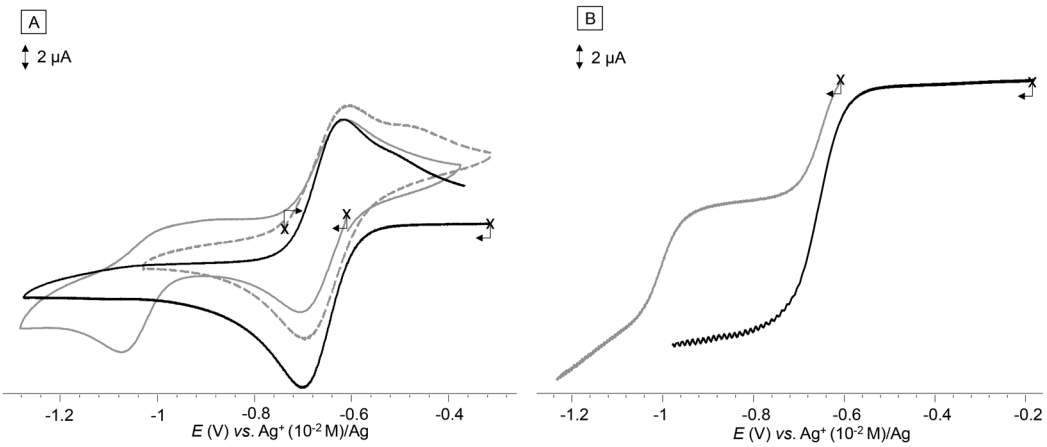

Fig. 7 (A) CV curves recorded for a 1 mM solution of $[\mathbf{1}^{VI}]$ in acetonitrile (+TBATFSI), before (black solid line) and after exhaustive electrolysis at E_{app} = −1 V (CPE, 1 e^{-} per mol) (dashed grey line), then 1h30 after addition of 1.0 molar equivalent of LutHCl (solid grey line). (B) RDE curve recorded for a 1 mM solution of $[\mathbf{1}^{VI}]$ in acetonitrile (+TBATFSI) (black solid line) and 1h30 after exhaustive electrolysis at E_{app} = −1 V (CPE, 1 e^{-} per mol) followed by 1.0 molar equivalent of LutHCl (solid grey line). CV and RDE curves were recorded at GC working electrodes (∅: 3 mm) either at 100 mV s^{-1} (CV) or 20 mV s^{-1} (RDE, 500 rpm). In all cases, the reference electrode was Ag^{+}(10^{-2} M)/Ag.

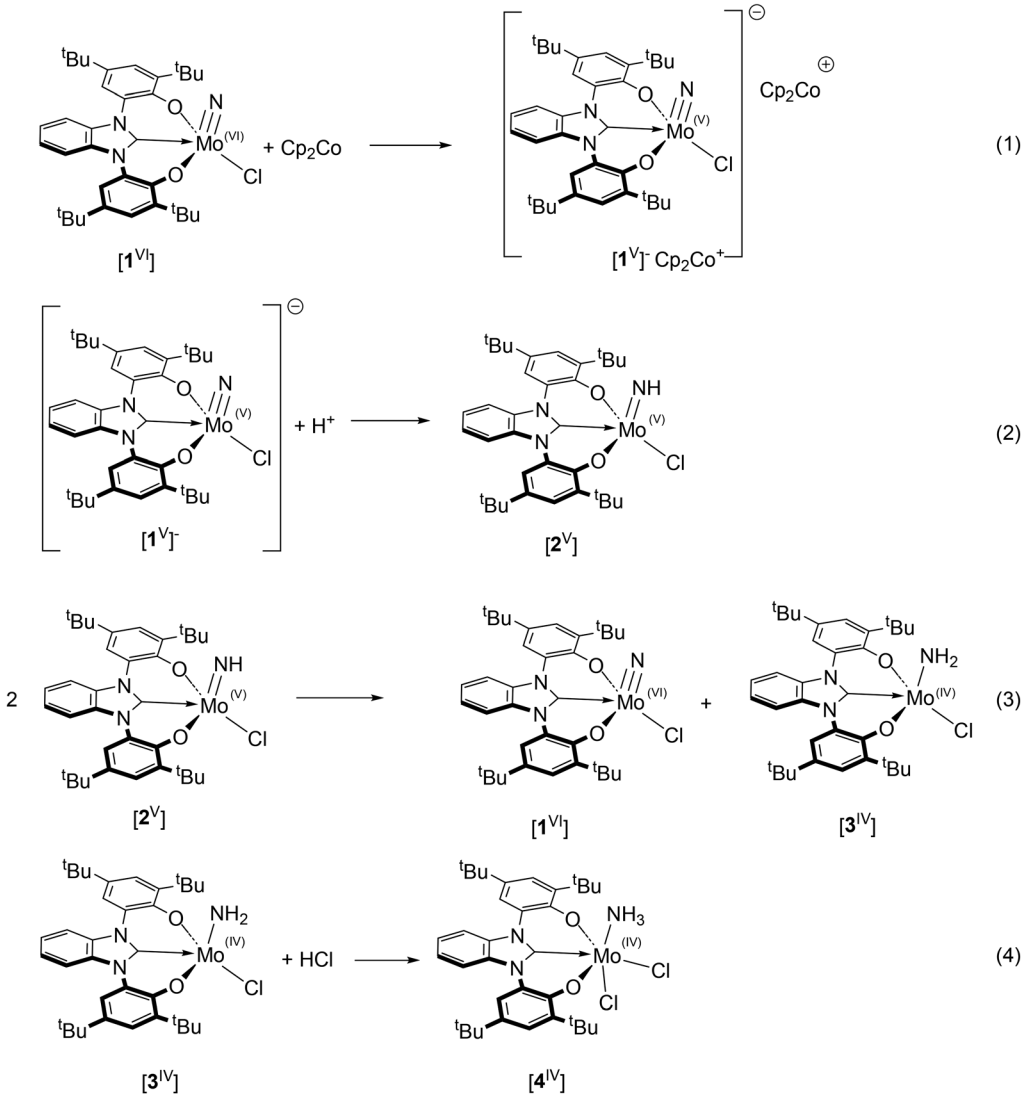

Scheme 3 Mechanism proposed for the reduction/protonation of nitrido complex [$\mathbf{1}^{VI}$].

LutHCl to afford complex [$\mathbf{2}^{V}$] [(OCO)Mo(═NH)Cl] (see eqn (1) and (2) in Scheme 3). This species is then transformed within an hour by a disproportionation reaction affording an equimolar mixture of the initial nitrido complex [$\mathbf{1}^{VI}$] [(OCO)Mo(≡N)Cl] and the amido complex [$\mathbf{3}^{IV}$] [(OCO)Mo(NH_2)Cl] (see eqn (3) in Scheme 3). The presence of the known complex [$\mathbf{1}^{VI}$] in the mixture is unambiguously demonstrated by the reduction wave observed at −0.69 V and by the absorption signal developing at 302 nm. On the other hand, the irreversible reduction wave at E_p = −1.09 V and the absorption signal at 440 are both attributed to the second product of the dismutation, the amido [$\mathbf{3}^{IV}$] complex incorporating an amido ligand linked to a Mo(IV) center. It should be mentioned that the proposed mechanism bears resemblance to previous results published by Yandulov and Schrock showing that the reduction of complex [($HIPTN_3N$)$Mo^{(V)}$═NH]$^+$ (with HIPT = hexaisopropylterphenyl) yields the corresponding species [($HIPTN_3N$)$Mo^{(VI)}$≡N] and [($HIPTN_3N$)$Mo^{(IV)}$–NH_2].[22]

Overall, the process triggered by addition of one electron and one proton leads to the consumption of only half of the starting nitride and to the formation of $\frac{1}{2}$ equivalent of the amide complex [$\mathbf{3}^{IV}$].

Formation and protonation of the amido complex [(OCO)Mo(NH_2)Cl] [$\mathbf{3}^{IV}$]

We then looked for experimental conditions allowing to achieve a complete conversion of [$\mathbf{1}^{VI}$] into [$\mathbf{3}^{IV}$]. These studies led us to establish that the remaining nitride complex, visible on the CV curves shown in Fig. 8, can be converted into [$\mathbf{3}^{IV}$] by subjecting the mixture to an additional reduction/protonation cycle involving further addition of 1 molar eq. of LutHCl (2 molar equivalents *versus* complex [$\mathbf{1}^{VI}$]) followed by CPE at −1.0 V (2 e^- per mole of [$\mathbf{1}^{VI}$]). The CV and RDV curves recorded after completion of this electrolysis (Fig. 8A, solid and dashed grey and black curves) reveal a disappearance of the first reduction wave at $E_{1/2}$ = −0.69 V in favor of an increase

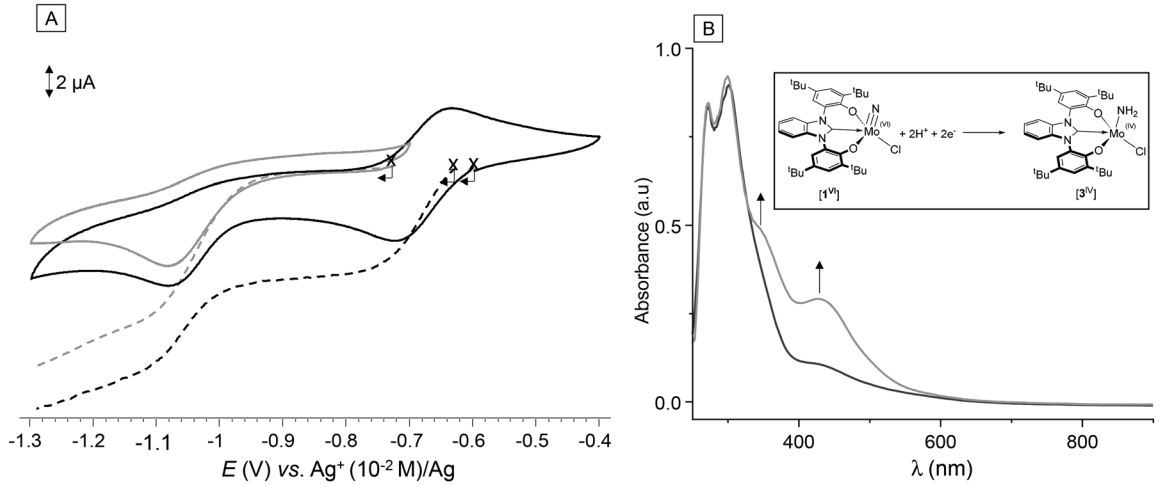

Fig. 8 (A) CV curves recorded on static (solid line) and rotating disk electrodes (dashed line) of the equimolar mixture of [$\mathbf{1}^{VI}$] and [$\mathbf{3}^{IV}$] (0.5 Mm each) in presence of 1 mM of LutHCl before (black) and after (grey) controlled potential electrolysis (E_{app} = −0.9 V) (B) Corresponding UV-visible absorption spectra. Optical path: 1 mm. Electrode GC (∅: 3 mm, RDE: 3 mm), reference: $Ag^+(10^{-2}$ M)/Ag, *v*: 100 mV s^{-1} (20 mV s^{-1} RDE), 500 rpm, counter electrode: Pt wire/carbon in acetonitrile + TBATFSI 0.1 M.

in the intensity of the second one at E_p = −1.09 V, attributed to the reduction of [$\mathbf{3}^{IV}$]. Accumulation of this complex in the mixture is also confirmed by an increase in the intensity of the band at λ_{max} = 440 nm (see solid grey and black curves in Fig. 8B). Overall, these (spectro)electrochemical data validate the disproportionation mechanism and show that the amido complex [$\mathbf{3}^{IV}$] can be produced quantitatively *in situ* after addition of 2 molar equivalents of e^-/H^+ to complex [$\mathbf{1}^{VI}$].

The full electrochemical signature of complex [$\mathbf{3}^{IV}$] recorded in acetonitrile (TBATFSI 0.1 M) is presented in Fig. S13. The curves recorded at a static carbon electrode include an intense irreversible wave at E_p = −1.09 V attributed to one electron reduction of [$\mathbf{3}^{IV}$] yielding an unstable Mo^{III} complex which evolves rapidly at the CV time scale. We then studied the protonation of [$\mathbf{3}^{IV}$] in the presence of LutHCl. The CV curves recorded in the cathodic domain before and after addition of 50 molar equivalents of LutHCl (*i.e.* conditions of electrocatalysis) on a millimolar solution of [$\mathbf{3}^{IV}$] in acetonitrile (Fig. S13) show that the protonation of [$\mathbf{3}^{IV}$] results in an increase in the intensity of the first reduction wave coming along with a slow shift of the pic potential (+50 mV after 1 hour of reaction). UV-visible absorption spectra recorded after the addition of 50 molar equivalents of LutHCl revealed a bathochromic shift of the main absorption band from 440 to 470 nm concomitent with its slow disappearance. These results thus support the conclusion that the amide (OCO)Mo(NH_2)Cl complex [$\mathbf{3}^{IV}$] can be protonated in the presence of excess LutHCl, to form [(OCO)Mo(NH_3)Cl_2] complex [$\mathbf{4}^{IV}$].

The experimental data discussed above are thus consistent with the mechanism shown in Scheme 4. Protonation of the amide moiety in [$\mathbf{3}^{IV}$] yields [$\mathbf{5}^{IV}$]$^+$, which subsequently undergoes the addition of a chloride ion on the metal center in trans position to the amine ligand to form the neutral ammonia complex [(OCO)Mo(NH_3)Cl_2] [$\mathbf{4}^{IV}$] (Scheme 4). Alternatively, coordination of Cl^- on the unsaturated Mo center in complex

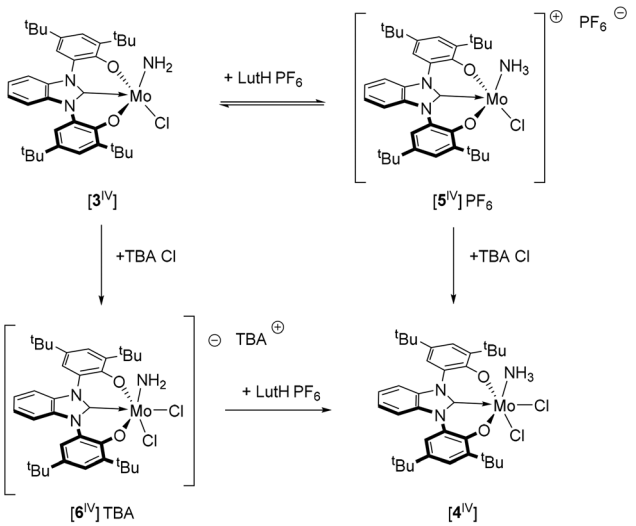

Scheme 4 Alternative pathways to complex [$\mathbf{4}^{IV}$].

[$\mathbf{3}^{IV}$] yields the anionic, hexacoordinated complex [$\mathbf{6}^{IV}$]$^-$, which is then readily protonated to afford [$\mathbf{4}^{IV}$]. These two mechanisms were evaluated by DFT calculations, *vide infra*.

Attempts at chemical synthesis of complex [$\mathbf{4}^{IV}$]: synthesis of complexes [$\mathbf{7}^{IV}$]$^-$ and [$\mathbf{8}^{IV-V}$]$^-$

Thanks to the understanding of the step-by-step transformations of the nitrido complex [$\mathbf{1}^{VI}$], we undertook the chemical synthesis of complex [$\mathbf{4}^{IV}$], which requires the addition of 3 protons and 2 electrons. In view of the results described in the preceding paragraphs, we used cobaltocene (Cp_2Co^{III}/Cp_2Co^{II} ~ −1.3 V *vs.* Ag^+/Ag), to achieve a selective one electron chemical reduction of complex [$\mathbf{1}^{VI}$].[43] The reaction between [$\mathbf{1}^{VI}$], two equivalents of Cp_2Co and three equivalents of LutHCl in

THF led to the precipitation of a salt which was removed by filtration (eqn (5) in Scheme 5). The remaining mixture was evaporated, washed with pentane and recrystallized form THF/heptane to give single crystals which could be subjected to X-ray diffraction analysis. The unexpected structure thus obtained (Fig. 9) features two metal centers bridged by a nitrogen atom.

The presence of a "N^{3-}" bridging ligand linking an (OCO)MoCl fragment and an (OCO)$MoCl_2^-$ fragment, led us to consider two Mo centers in different oxidation states. The Mo^1–N and Mo^2–N bond lengths are very different at 2.020(2) Å and 1.702(2) Å respectively. The latter bond distance is only slightly elongated compared to the MoN in the nitride complexes [(OCO)MoNCl] [$\mathbf{1}^{VI}$] (1.649(1) Å) and [(OCO)MoNCl]$^-$ [$\mathbf{1}^{V}$]$^-$ (1.627(7) Å) while the Mo–Cl bond is almost identical to the one measured in the reduced complex [(OCO)MoNCl]$^-$ [$\mathbf{1}^{V}$]$^-$ (2.434(8) Å *vs.* 2.447(2) Å in [$\mathbf{1}^{V}$]$^-$). All together, these data support the existence of a Mo≡N bond in complex [$\mathbf{8}^{V-IV}$]$^-$. The much longer Mo1–N bond, at 2.020(2) Å is more compatible with a donor–acceptor interaction. Overall, this bimetallic μ-N bridged structure is an assembly of one nitride-Mo^V fragment [$OCOMo^{(V)}NCl$]$^-$ which acts as a donor to the unsaturated Mo^{IV} fragment [$OCOMoCl_2$]. Notably, the Mo–Cl bond in *trans* position (2.497(8) Å) to the strong N donor is elongated *vs.* the Mo–Cl *cis* (2.444(8) Å).

Furthermore, the *in situ* generation of an (OCO)$MoCl_2$ fragment demonstrates the possibility of easily functionalizing the N center of the nitrido complex by reduction/protonation and displacing the NH_3 ligand (Scheme 5). It also shows that the N center of the anionic nitrido complex [$\mathbf{1}^{V}$]$^-$ is a very suitable ligand for an unsaturated Mo^{IV} center, which in turn precludes subsequent transformations.

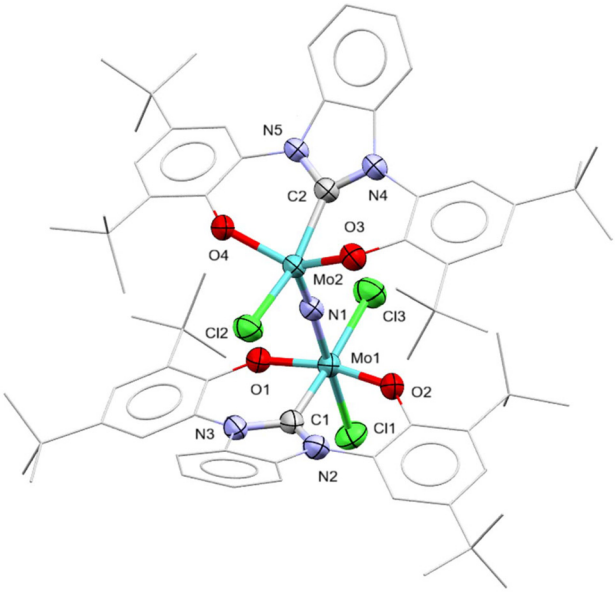

Fig. 9 X-ray structure of anionic part of [$\mathbf{8}^{V-IV}$]$^-$·Cp_2Co^+. Ellipsoids are shown with a 50% probability. Hydrogen atoms and cobalticinium cation are omitted for clarity.

We reasoned that the formation of this bridged N dimer [$\mathbf{8}^{V-IV}$]$^-$ could result from two undesirable facts. Firstly, Cp_2Co is a reducing agent powerful enough to reduce the *in situ* generated amido complex [$\mathbf{3}^{IV}$] into [$\mathbf{3}^{III}$], which seems to be unstable in our experimental conditions (see the irreversible reduction wave at −1.1 V in Fig. 8). We therefore sought to achieve a more selective chemical reduction using a milder

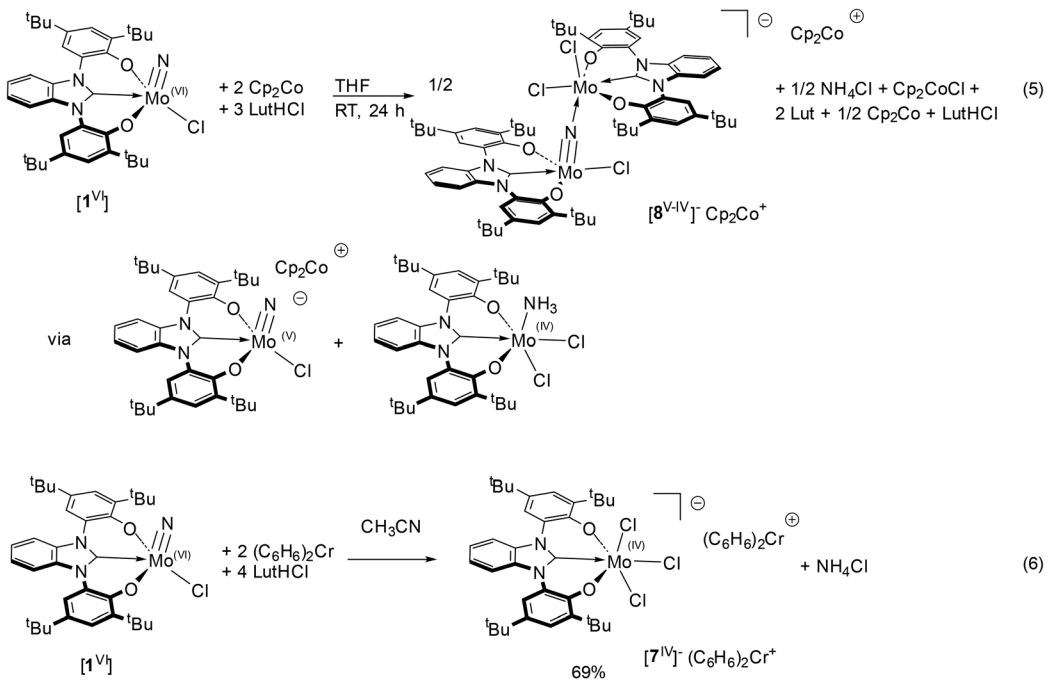

Scheme 5 Synthesis of complexes [$\mathbf{7}^{IV}$]$^-$ and [$\mathbf{8}^{V-IV}$]$^-$ by chemical reduction of complex [$\mathbf{1}^{VI}$].

reducing agent such as $(C_6H_6)_2Cr$ ($E°[(C_6H_6)_2Cr^{II}/(C_6H_6)_2Cr^{III+}]$ = −1.1 V in CH_2Cl_2 *vs.* Cp_2Fe).[43]

Thus, reacting [**1**^{VI}] with two equivalents of $(C_6H_6)_2Cr$ and four equivalents of LutHCl in CH_3CN led to the formation of a precipitate. Filtration and slow evaporation of the solution afforded single crystals of complex [**7**^{IV}]$^-$ $(C_6H_6)_2Cr^+$ obtained in a good 69% yield. The structure determined by X-ray diffraction corresponds to an octahedral trichloro Mo^{IV} anionic complex (Fig. 10), the existence of which had previously been postulated on the ground of experimental data.

The negative charge of the complex and the +IV oxidation state of the Mo center in [**7**^{IV}]$^-$ $(C_6H_6)_2Cr^+$ were confirmed by ESR measurements showing an intense signal centered at g = 1.99 exhibiting hyperfine coupling constants, characteristic of a bis(benzene)chromium cation (Fig. S21).[46] Attempts to characterize [**7**^{IV}]$^-$$(C_6H_6)_2Cr^+$ by electrochemical methods have been seriously limited by the presence of the bis(benzene)chromium cation whose signature overlaps with that of the Mo complex. The CV curves recorded in the anodic domain for a solution of [**7**^{IV}]$^-$ (0.5 mM) in acetonitrile (TBATFSI 0.1 M) (Fig. S14) however displays a reversible oxidation wave at $E_{1/2}$ = −0.18 V matching the one obtained one hour after the addition of 50 molar equivalents of LutHCl to a solution of [**3**^{IV}].

Theoretical calculations

DFT (PBE0-D3) calculations were carried out to gain further insight into the mechanism (see SI for computational details). In each case, the different spin states for the species were evaluated (singlet or triplet on one side, or doublet or quartet in other cases). The structures reported correspond to the most stable case in each situation (see computation details in SI, Table S12 with the relative energies of the different spin states). Our goal was also to identify the step(s) preventing the establishment of an efficient electrocatalytic process.

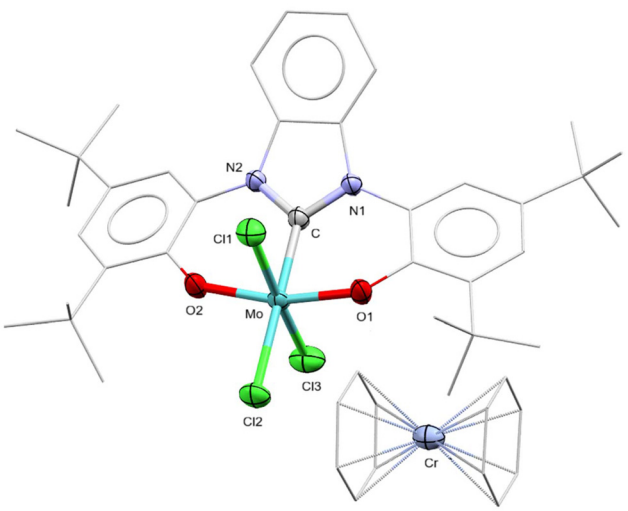

Fig. 10 Molecular structure of [**7**^{IV}]$^-$$(C_6H_6)_2Cr^+$ determined by single crystal X-ray diffraction analyses. Hydrogen atoms are omitted for clarity. 50% thermal ellipsoids are show.

The one-electron reduction of the starting nitrido complex [**1**^{VI}] (S = 0) with Cp_2Co was calculated at ΔG = −8.8 kcal mol^{-1} (Scheme 6). Further calculations revealed that the protonation of the anionic complex [**1**^{V}]$^-$ with LutH$^+$ yielding the imido complex [**2**^{V}] ($S = \frac{1}{2}$) is an equilibrium, as attested by the low positive ΔG = +1.9 kcal mol^{-1}. Subsequent reactions are driven by the dismutation process. Indeed, formation of [**1**^{VI}] + [**3**^{IV}] from two complexes [**2**^{V}] is mildly exergonic, with ΔG = −4.3 kcal mol^{-1}. Complex [**3**^{IV}] is computed to be more stable in the triplet state (S = 1). Two pathways were then evaluated to reach the ammonia complex [**4**^{IV}] upon addition of LutHCl, either protonation of complex [**3**^{IV}] followed by coordination of Cl$^-$ or the reverse. This process is overall significantly exergonic (ΔG = −15.1 kcal mol^{-1}). Protonation of complex [**3**^{IV}] at the N center of the amido moiety with LutH$^+$ leads to complex [**5**^{IV}]$^+$ (S = 0) in an endergonic fashion, ΔG = 6.1 kcal mol^{-1}. Subsequent Cl$^-$ coordination on the unsaturated pentacoordinated complex is then computed to be strongly exergonic, with ΔG = −21.2 kcal mol^{-1}, forming the hexacoordinated complex [**4**^{IV}] in its singlet state. Alternatively, chloride coordination on the coordinatively unsaturated complex [**3**^{IV}] forms the anionic complex [**6**^{IV}]$^-$ in a favorable fashion (ΔG = −4.8 kcal mol^{-1}), followed by protonation, also exergonic (ΔG = −10.3 kcal mol^{-1}). This second pathway thus appears more favorable. It is interesting to note that the coordination of chloride increases the electron density at the NH_2 moiety, rendering it more basic. Thus, the added anionic charge is not compensated by the strong electron withdrawing character of the Cl atom. At this stage, three N–H bonds have been created upon addition of 2 electrons and 3 LutHCl. Most notably, this sequence of events is exergonic, which rationalizes the experimental findings presented above, demonstrating that NH_3 formation from the (OCO)MoNCl Mo-nitride complex [**1**^{VI}] is readily achieved. In order to achieve a catalytic cycle, ammonia needs to be displaced from the Mo center for subsequent N_2 coordination. Functionalization of N_2 would then occur *via* the dissociative pathway, implying N_2 splitting, or associative (Schrock type) (Scheme 7).

The evaluation of the different paths was therefore studied by calculation. At first, NH_3 substitution reactions by Cl$^-$ and N_2 at the Mo(IV) oxidation state were computed. Complex [**4**^{IV}] being hexacoordinated, a dissociation of NH_3 is a prerequisite to substitution. As shown in Scheme 8, the unsaturated complex [**A**] is computed at ΔG = 22.0 kcal mol^{-1} higher. Subsequent coordination of N_2 is then only marginally favorable (ΔG = −1.9 kcal mol^{-1}), making the overall exchange NH_3 to N_2 unfavorable by 20.1 kcal mol^{-1}. Halide anions Cl$^-$ being potential competitive ligands, their coordination was computed. Most interestingly, it is even favored compared to NH_3 coordination, with a ΔG = −0.7 kcal mol^{-1}. The overall reaction of complex [**6**^{IV}] with LutHCl yielding [**7**^{IV}]$^-$, NH_4^+ and Lut was computed almost thermo neutral (ΔG = +0.3 kcal mol^{-1}). These results are therefore in agreement with the isolation of the [(OCO)MoCl$_3$]$^-$ complex (*vide infra*). In conclusion, coordination of N_2 at the Mo(IV) oxidation state is clearly unfavored *vs.* both Cl$^-$ and NH_3. Reduction of the Mo(IV)(N_2) complexes into Mo(III) was thus computed, with either Cp_2Co ($E°$ =

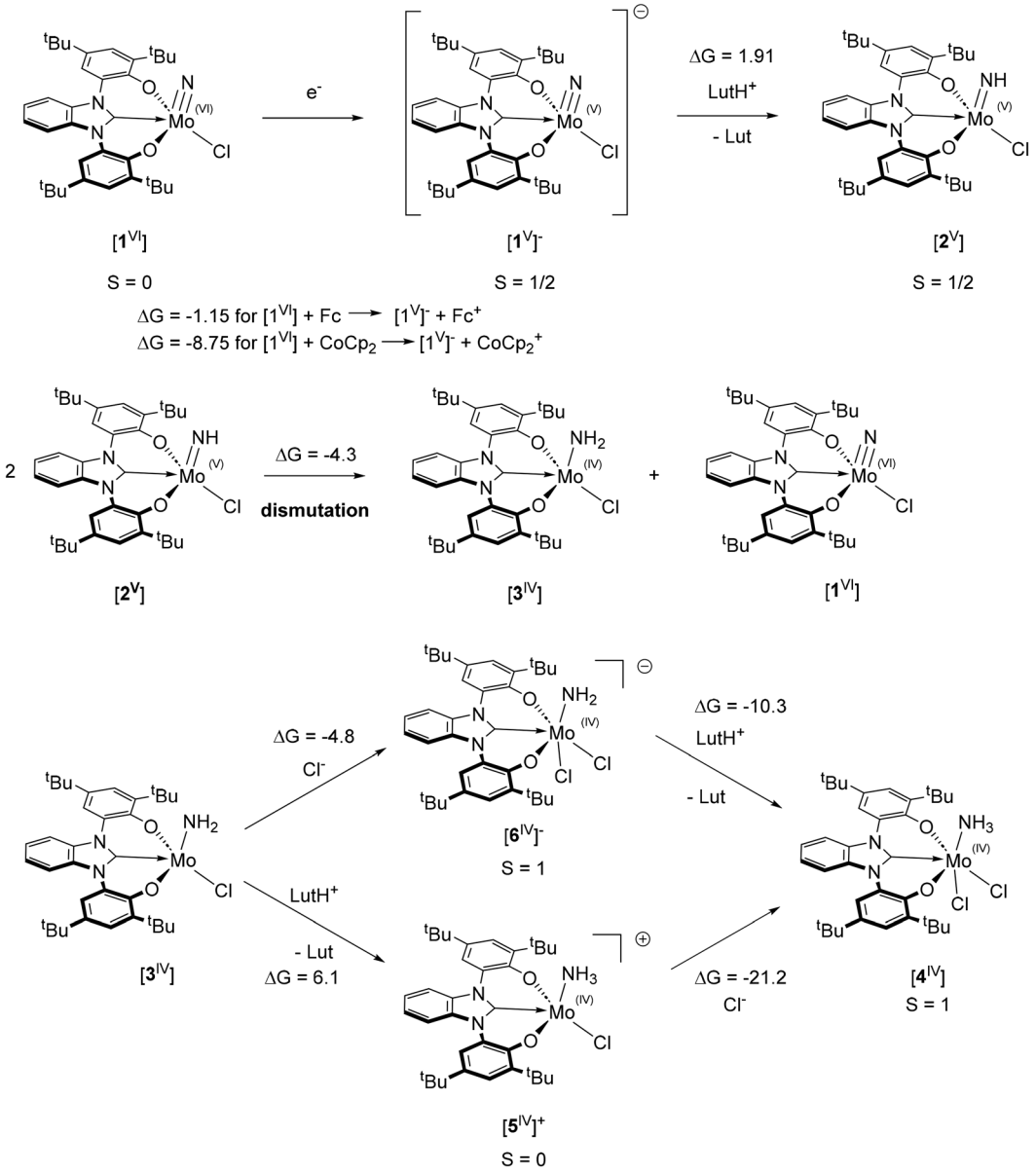

Scheme 6 Formation of ammonia upon reaction of [1^{VI}] with 2 electrons and 3 LutHCl.

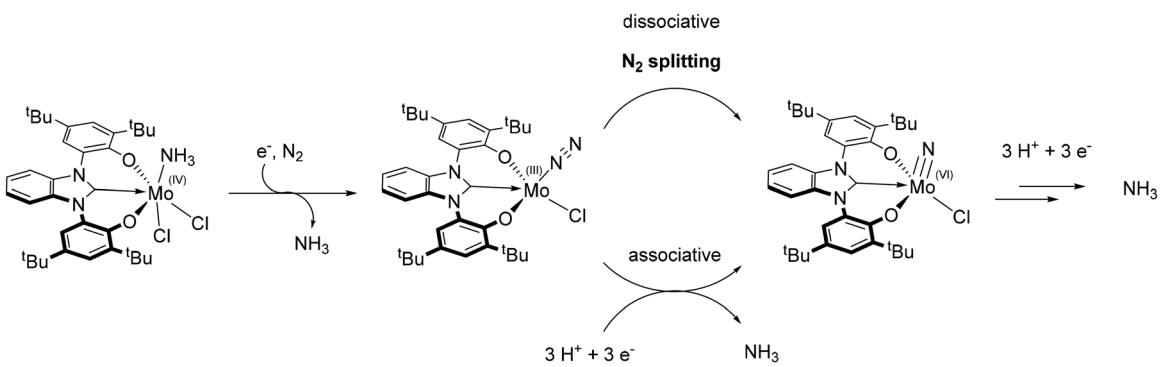

Scheme 7 illustration of the mechanistic pathways for N_2 fixation from complex [4^{IV}].

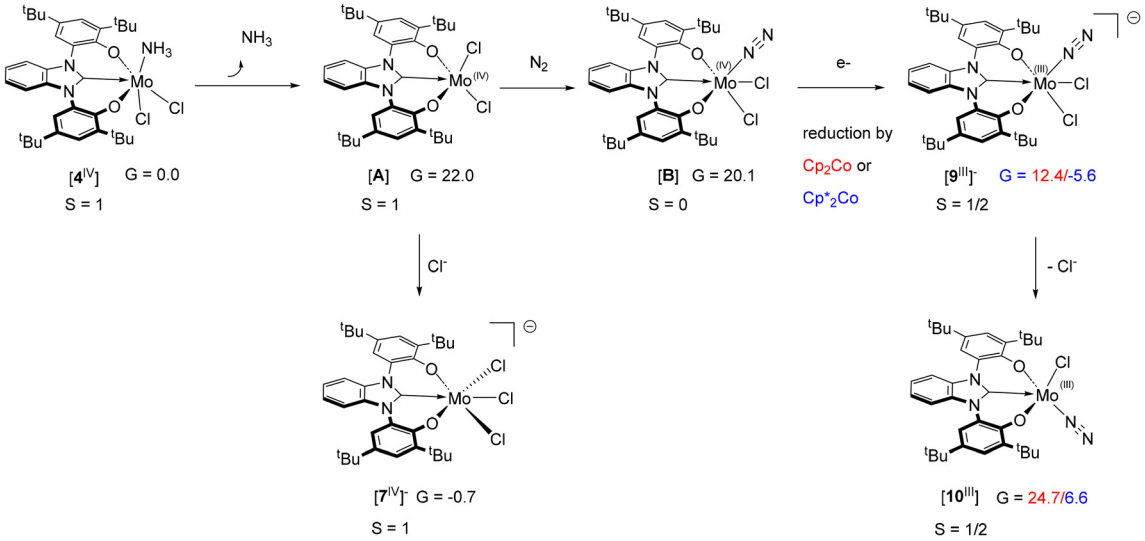

Scheme 8 NH_3 to N_2 substitution at Mo(IV) and Mo(III) oxidation states.

−1.33 V in CH_2Cl_2 *vs.* Fc) and Cp^*_2Co ($E°$ = −1.91 V in CH_3CN *vs.* Fc) (Scheme 8).[43] Interestingly, reduction of complex [**B**] [(OCO)$MoCl_2(N_2)$] by both agents is exergonic, with ΔG = −7.7 kcal mol^{-1} with Cp_2Co, and very exergonic ΔG = −25.7 kcal mol^{-1} with Cp^*_2Co. Most importantly, this reduction step now provides a viable NH_3 to N_2 substitution, with an exergonic transformation [$\mathbf{4}^{IV}$] + Cp^*_2Co + N_2 → [$\mathbf{9}^{III}$]$^-$ + NH_3 + $Cp^*_2Co^+$ (ΔG = −5.6 kcal mol^{-1}). Overall, it rationalizes the fact that three electrons and three protons are needed to functionalize the N center in complex [$\mathbf{1}^{VI}$], followed by the substitution of NH_3 by N_2. In this case also, coordination of the Cl^- ligand to form the hexacoordinated complex [$\mathbf{9}^{III}$]$^-$ is favored over the unsaturated pentacoordinated complex [$\mathbf{10}^{III}$], by 12.3 kcal mol^{-1}. It is not surprisingly less so than at the Mo (IV) oxidation state (favored by 22.7 kcal mol^{-1}).

Overall, the DFT calculations fully rationalize our experimental findings. Namely, they support a facile dismutation process from the imido complex Mo(NH)(V) [$\mathbf{2}^{V}$], leading to an overall efficient 2 electrons 2 proton transfers forming the amido complex [$\mathbf{3}^{IV}$] Mo(IV). Subsequent reaction with one and two eq. of LutHCl is favorable. The first step generates coordinated NH_3 while the second one leads to the corresponding (OCO)$MoCl_3^-$ complex and NH_4^+ formation. Interestingly, chloride Cl^- is as good a ligand as NH_3 for the (OCO)$MoCl_2$ fragment. Coordination of N_2 becomes only possible upon one electron reduction of the Mo(IV) into Mo(III).

Reduction of complex [$\mathbf{7}^{IV}$]$^-$

These theoretical studies prompted us to investigate the reduction of [$\mathbf{7}^{IV}$]$^-$·$Cr(C_6H_6)_2^+$ in order to evaluate the ability of the *in situ* generated Mo(III) center to coordinate N_2. This presents a technical issue as $Cr(C_6H_6)_2$ would also be generated by reduction. We identified the one electron oxidized neutral complex [$\mathbf{7}^{V}$], featuring a Mo(V) center, as appropriate precursor. This species was synthesized in 71% yield following the strategy reported recently by Hu, relying on the reaction of complex [$\mathbf{1}^{VI}$] with PCl_5.[21] The electrochemical signature of [$\mathbf{7}^{V}$] is shown in Fig. S15. The CV curve recorded in ACN exhibits a fully reversible reduction wave around −0.2 V, which is in agreement with the expected stability of the electrogenerated species [$\mathbf{7}^{IV}$]$^-$. Most importantly, this wave is also found to be identical to the first reversible oxidation observed on the voltammogram shown in Fig. S14 obtained with complex [$\mathbf{7}^{IV}$]$^-$. An irreversible reduction is also observed at E_p ∼ −1.30 V which results from chemical reactions following the formation of [$\mathbf{7}^{III}$]$^{2-}$, most likely following the release of Cl^-.

Several chemical agents and conditions were tested to reduce [$\mathbf{7}^{V}$] by two electrons and yield the Mo(III) complexes [$\mathbf{9}^{III}$]$^-$ [(OCO)$Mo(N_2)Cl_2$]$^-$ or [$\mathbf{10}^{III}$] [(OCO)$Mo(N_2)$Cl]. In all cases, several complexes were formed, as attested by the ^1H NMR spectra recorded for the crude mixtures. The most selective reaction was obtained between complex [$\mathbf{7}^{V}$] and 2 eq. of Na/Hg, under N_2, in 2-Me-THF for 12 h. Under these conditions, 58% of the Mo–Mo dimer [$\mathbf{11}^{III}$] featuring a triple bond was isolated (Scheme 9). The crystal structure of this complex was reported by Hohloch while this work was underway.[34] Note that in their case, this complex was obtained in <2% yield by reduction of their complex [(OCO)Mo(N)Cl] with Cp^*_2Co. Most importantly, the formation of this complex demonstrates that the two electrons reduction of [(OCO)$MoCl_3$] [$\mathbf{7}^{V}$] Mo(V), results in the expected elimination of Cl^- to form the desired "(OCO)MoCl" Mo(III) fragment. At this stage, dimerization occurs rather than N_2 coordination, creating a dead-end that prevents the existence of a catalytic process.

Closing the loop to complex [$\mathbf{1}^{VI}$] *via* N_2 splitting: DFT calculations

Having identified experimentally a first bottleneck that prevents efficient N_2-to-NH_3 electrocatalysis using complex [$\mathbf{1}^{VI}$], we evaluated by theoretical calculations the N_2 splitting from

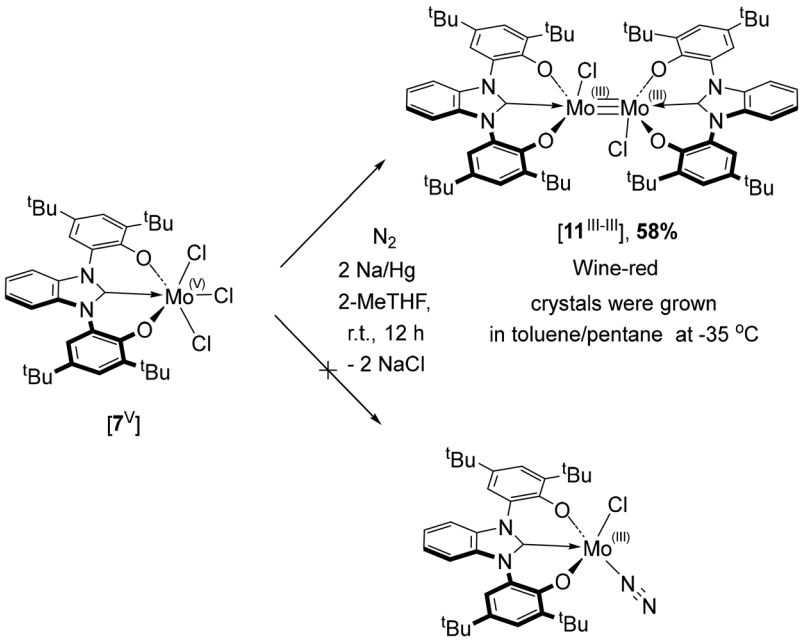

Scheme 9 Formation of [$\mathbf{11}^{\mathrm{III-III}}$] by reduction of [$\mathbf{7}^{\mathrm{V}}$].

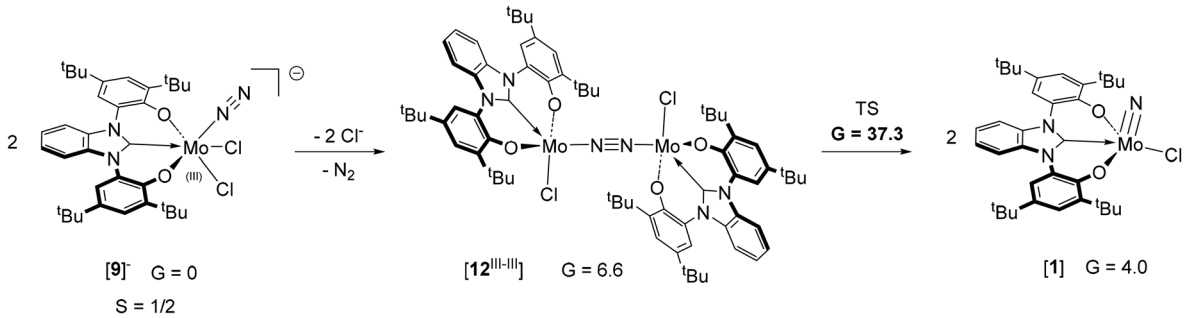

Scheme 10 Computations of the N_2 splitting process.

two "(OCO)MoCl" Mo(III) fragments, to yield complex [$\mathbf{1}^{\mathrm{VI}}$] (Scheme 10). As previously highlighted, it involves an overall six electron transfer between two metal centers and the N_2 moiety, thus three electrons per M center. Starting from two equivalents of [$\mathbf{9}^{\mathrm{III}}$]$^-$, formation of the dimer [$\mathbf{11}^{\mathrm{III-III}}$] would result from the elimination of two Cl^- and the dissociation of one N_2 molecule. This process was found to be endergonic by 6.6 kcal mol^{-1}. From the dimer, the splitting of N_2 is computed to be exergonic (ΔG = −2.6 kcal mol^{-1}), and thus endergonic from [$\mathbf{9}^{\mathrm{III}}$]$^-$ (ΔG = by 4.0 kcal mol^{-1}). This would still be acceptable for a catalytic process, however a high energy barrier for the splitting was computed (ΔG = 30.7 kcal mol^{-1} from the dimer, and ΔG = 37.3 kcal mol^{-1} above complex [$\mathbf{9}^{\mathrm{III}}$]$^-$), which clearly precludes a thermal process under mild conditions.

These computations therefore strongly suggest that if a pathway for N_2 functionalization exists with this (OCO)MoCl type fragment, as demonstrated by the group of Hu,[21] it does not involve N_2 splitting, but a more classical "Schrock" cycle, involving sequential electron/electrophile (or radical) addition on coordinated N_2.

Conclusions

We have reported here the synthesis of a molybdenum nitride bis-aryloxycarbene complex [(OCO)MoNCl] [$\mathbf{1}^{\mathrm{III}}$]. This complex was evaluated as a possible entry point into an electro-catalytic cycle for N_2-to-NH_3, using LutHOTf as proton source and controlled potential. The poor catalytic efficiency of this process prompted us to study in depth the elementary steps of the H^+/e^- transfers. By electrochemistry we have identified a facile, dismutation process from the [(OCO)Mo(NH)Cl] intermediate Mo(V), leading to reformation of the starting complex [$\mathbf{1}^{\mathrm{VI}}$] together with the amido complex [(OCO)Mo(NH_2)Cl] Mo(IV) [$\mathbf{3}^{\mathrm{IV}}$]. Following this mechanism, reduction of complex [$\mathbf{1}^{\mathrm{VI}}$] by

two electrons (CPE) in the presence of 2 equivalents of acid results in quantitative formation of the [(OCO)Mo(NH_2)Cl] Mo(IV) complex. Subsequent addition of LutHCl is also facile, leading to the ammonia complex [(OCO)Mo(NH_3)Cl_2] Mo(IV) [$\mathbf{4}^{IV}$]. At this point, functionalization of the N of the nitride by 3 LutHCl/2 electrons is achieved. Closing the catalytic cycle to reform the nitride complex [$\mathbf{1}^{VI}$] proved very unfavorable for two different reasons. First, the presence of Cl^- in the medium, as in catalytic conditions, would favor NH_3 displacement to yield complex [(OCO)$MoCl_3$]$^-$ [$\mathbf{7}^{IV}$]$^-$, which is readily reduced by one electron to form the highly unsaturated "(OCO)MoCl" fragment. One of the unfavorable evolutions of this fragment, in terms of catalysis, is to dimerize to form the very stable dimer [(OCO)MoCl]$_2$ Mo(III) [$\mathbf{11}^{III-III}$], which we have isolated. Alternatively, ammonia can be substituted by N_2 to form the [(OCO)Mo(N_2)Cl_2] Mo(IV). Reduction of this complex by one electron would yield the dinitrogen complex [(OCO)Mo(N_2)Cl] Mo(III). Direct splitting of N_2 from the corresponding [(OCO)MoCl]$_2$(μ-N_2) bridging dimer to form (OCO)MoNCl [$\mathbf{1}^{VI}$] was computed to be prohibitively high in energy. Reaching the nitride complex *via* N_2 splitting is not a prerequisite of N_2 functionalization using the (OCO) ligand, as Hu has demonstrated catalytic silylation of N_2 using a similar (OCO)MoNCl complex. This process thus most likely occurs *via* associative mechanism.

Our work therefore provides key understanding on the elementary steps of the H^+/e^- transfer from the "(OCO)MoCl/N_2" system. Efforts are currently focused experimentally and theoretically on ligand design to prevent dimerization of the "(OCO)MoCl" intermediate, as well as to favor the N_2 splitting, *i.e.* to decrease the energy of the corresponding transition state, as functionalization of the nitride to NH_3 is then facile.

Author contributions

T. P.: methodology, investigation, writing – original draft. X. W.: investigation, formal analysis. J. B.: investigation. S. A.: investigation. M. D.: investigation. S. B.: formal analysis. N. S.-M.: formal analysis. M. B.: formal analysis. E. C.: DFT calculations. C. B.: writing draft, supervision. N. M.: DFT calculations, writing draft, supervision.

Conflicts of interest

There are no conflicts to declare.

Data availability

The data supporting the findings of this study are available in the supplementary information (SI). Supplementary information is available. See DOI: https://doi.org/10.1039/d6qi00081a.

CCDC 2515875 ([$\mathbf{1}^{VI}$]), 2515876 ([$\mathbf{1}^{V}$]$^-$), 2515877 ([$\mathbf{8}^{V-IV}$]$^-$), 2515878 ([$\mathbf{7}^{IV}$]$^-$) and 2515879 ([$\mathbf{7}^{V}$]) contain the supplementary crystallographic data for this paper.[47a–e]

Acknowledgements

Financial support from CNRS, ANR (ANR-23-CE07-0049-02, Post-doc funding for XW and SA) and from the Ecole Normale Supérieure de Lyon (Projet emergence, PhD funding to TP) is acknowledged. This work was performed using HPC resources from CALMIP (Grant 2021-P1310). The NMR service of the ICT (UAR 2599) is acknowledged. The authors thank Fatima Akhssas Pioche for her help in the electrochemical characterization of complex [$\mathbf{7}^{V}$].

References

1 Y. Roux, C. Duboc and M. Gennari, Molecular Catalysts for N $_2$ Reduction: State of the Art, Mechanism, and Challenges, *ChemPhysChem*, 2017, **18**, 2606–2617.
2 M. J. Chalkley, M. W. Drover and J. C. Peters, Catalytic N2-to-NH3 (or -N2H4) Conversion by Well-Defined Molecular Coordination Complexes, *Chem. Rev.*, 2020, **120**, 5582–5636.
3 Y. Tanabe and Y. Nishibayashi, Comprehensive insights into synthetic nitrogen fixation assisted by molecular catalysts under ambient or mild conditions, *Chem. Soc. Rev.*, 2021, **50**, 5201–5242.
4 Y. Tanabe and Y. Nishibayashi, Recent advances in catalytic nitrogen fixation using transition metal–dinitrogen complexes under mild reaction conditions, *Coord. Chem. Rev.*, 2022, **472**, 214783.
5 J. Chatt, A. J. Pearman and R. L. Richards, The reduction of mono-coordinated molecular nitrogen to ammonia in a protic environment, *Nature*, 1975, **253**, 39–40.
6 J. Chatt, J. R. Dilworth and R. L. Richards, Recent advances in the chemistry of nitrogen fixation, *Chem. Rev.*, 1978, **78**, 589–625.
7 M. Hidai and Y. Mizobe, Recent Advances in the Chemistry of Dinitrogen Complexes, *Chem. Rev.*, 1995, **95**, 1115–1133.
8 T. Personeni, M. Duquesnoy, C. Bucher and N. Mézailles, Electrochemical reduction of N2 in mild conditions using redox or chemical catalysis: towards alternatives to the Haber-Bosch process?, *Coord. Chem. Rev.*, 2026, **557**, 217726.
9 D. V. Yandulov and R. R. Schrock, Catalytic Reduction of Dinitrogen to Ammonia at a Single Molybdenum Center, *Science*, 2003, **301**, 76–78.
10 C. E. Laplaza and C. C. Cummins, Dinitrogen Cleavage by a Three-Coordinate Molybdenum(lil) Complex, *Science*, 1995, **268**, 861–863.
11 Q. J. Bruch, S. Malakar, A. S. Goldman and A. J. M. Miller, Mechanisms of Electrochemical N $_2$ Splitting by a

Molybdenum Pincer Complex, *Inorg. Chem.*, 2022, **61**, 2307–2318.

12 R. S. van Alten, F. Wätjen, S. Demeshko, A. J. M. Miller, C. Würtele, I. Siewert and S. Schneider, (Electro–)chemical Splitting of Dinitrogen with a Rhenium Pincer Complex, *Eur. J. Inorg. Chem.*, 2020, **2020**, 1402–1410.

13 M. J. Chalkley, T. J. Del Castillo, B. D. Matson and J. C. Peters, Fe-Mediated Nitrogen Fixation with a Metallocene Mediator: Exploring pK_a Effects and Demonstrating Electrocatalysis, *J. Am. Chem. Soc.*, 2018, **140**, 6122–6129.

14 B. M. Lindley, R. S. van Alten, M. Finger, F. Schendzielorz, C. Würtele, A. J. M. Miller, I. Siewert and S. Schneider, Mechanism of Chemical and Electrochemical N_2 Splitting by a Rhenium Pincer Complex, *J. Am. Chem. Soc.*, 2018, **140**, 7922–7935.

15 G. P. Connor, D. Delony, J. E. Weber, B. Q. Mercado, J. B. Curley, S. Schneider, J. M. Mayer and P. L. Holland, Facile conversion of ammonia to a nitride in a rhenium system that cleaves dinitrogen, *Chem. Sci.*, 2022, **13**, 4010–4018.

16 T. Munisamy and R. R. Schrock, An electrochemical investigation of intermediates and processes involved in the catalyticreduction of dinitrogen by [HIPTN3N]Mo (HIPTN3N = (3,5-(2,4,6-iPr3C6H2)2C6H3NCH2CH2)3N), *Dalton Trans.*, 2012, **41**, 130–137.

17 E. A. Boyd, H. Jung and J. C. Peters, Samarium as a Catalytic Electron-Transfer Mediator in Electrocatalytic Nitrogen Reduction to Ammonia, *J. Am. Chem. Soc.*, 2025, **147**, 4695–4700.

18 P. Garrido-Barros, J. Derosa, M. J. Chalkley and J. C. Peters, Tandem electrocatalytic N2 fixation via proton-coupled electron transfer, *Nature*, 2022, **609**, 71–76.

19 T. Personeni, B. Rialland, I. Benaissa, S. Bennaamane, L. Khrouz, A. Mulas, M. Fustier-Boutignon, E. Clot, N. Mézailles and C. Bucher, Catalytic Activity and Mechanistic Investigations of the Nitrido Molybdenum Complex [(PPP)Mo(≡N)(I)] in the Electrochemical Reduction of N2, *Inorg. Chem.*, 2025, **64**, 8863–8874.

20 A. F. Ibrahim, P. Garrido-Barros and J. C. Peters, Electrocatalytic Nitrogen Reduction on a Molybdenum Complex Bearing a PNP Pincer Ligand, *ACS Catal.*, 2023, **13**, 72–78.

21 Z. Li, C. Liu, J. An, X. Wang and S. Hu, Catalytic Dinitrogen Reduction to Silylamines by Molybdenum Nitride Complexes Bearing a Diphenolate N-Heterocyclic Carbene Ligand, *ACS Catal.*, 2024, **14**, 6558–6564.

22 D. V. Yandulov and R. R. Schrock, Studies Relevant to Catalytic Reduction of Dinitrogen to Ammonia by Molybdenum Triamidoamine Complexes, *Inorg. Chem.*, 2005, **44**, 1103–1117.

23 F. Studt and F. Tuczek, Energetics and Mechanism of a Room-Temperature Catalytic Process for Ammonia Synthesis (Schrock Cycle): Comparison with Biological Nitrogen Fixation, *Angew. Chem., Int. Ed.*, 2005, **44**, 5639–5642.

24 J. J. Curley, E. L. Sceats and C. C. Cummins, A Cycle for Organic Nitrile Synthesis via Dinitrogen Cleavage, *J. Am. Chem. Soc.*, 2006, **128**, 14036–14037.

25 Y. Ashida, T. Mizushima, K. Arashiba, A. Egi, H. Tanaka, K. Yoshizawa and Y. Nishibayashi, Catalytic production of ammonia from dinitrogen employing molybdenum complexes bearing N-heterocyclic carbene-based PCP-type pincer ligands, *Nat. Synth.*, 2023, **2**, 635–644.

26 Y. Ashida, K. Arashiba, K. Nakajima and Y. Nishibayashi, Molybdenum-catalysed ammonia production with samarium diiodide and alcohols or water, *Nature*, 2019, **568**, 536–540.

27 S. Bellemin-Laponnaz and S. Dagorne, Group 1 and 2 and Early Transition Metal Complexes Bearing N-Heterocyclic Carbene Ligands: Coordination Chemistry, Reactivity, and Applications, *Chem. Rev.*, 2014, **114**, 8747–8774.

28 C. Romain, L. Brelot, S. Bellemin-Laponnaz and S. Dagorne, Synthesis and Structural Characterization of a Novel Family of Titanium Complexes Bearing a Tridentate Bis-phenolate-N-heterocyclic Carbene Dianionic Ligand and Their Use in the Controlled ROP of *rac*-Lactide, *Organometallics*, 2010, **29**, 1191–1198.

29 S. Bellemin-Laponnaz, R. Welter, L. Brelot and S. Dagorne, Synthesis and structure of V(v) and Mn(iii) NHC complexes supported by a tridentate bis-aryloxide-N-heterocyclic carbene ligand, *J. Organomet. Chem.*, 2009, **694**, 604–606.

30 E. Despagnet-Ayoub, L. M. Henling, J. A. Labinger and J. E. Bercaw, Addition of a phosphine ligand switches an N-heterocyclic carbene-zirconium catalyst from oligomerization to polymerization of 1-hexene, *Dalton Trans.*, 2013, **42**, 15544–15547.

31 J. Frey, S. Azar, S. Dagorne and S. Bellemin-Laponnaz, Bis (phenolate) N-Heterocyclic Carbene [OCO] Pincer Ligands: A Unique Family for the Stabilization of Transition Metal Centers and Main Group Elements, *ChemistryEurope*, 2026, **4**, e202500283.

32 D. M. T. Chan, M. H. Chisholm, K. Folting, J. C. Huffman and N. S. Marchant, Trialkoxynitridomolybdenum compounds: (RO)3Mo.ident.N. Preparation, structures (R = tert-Bu and iso-Pr), and comparisons with a tungsten analog (R = tert-Bu), *Inorg. Chem.*, 1986, **25**, 4170–4174.

33 P. Chaudhuri, M. Hess, J. Müller, K. Hildenbrand, E. Bill, T. Weyhermüller and K. Wieghardt, Aerobic Oxidation of Primary Alcohols (Including Methanol) by Copper(ii)– and Zinc(ii)–Phenoxyl Radical Catalysts, *J. Am. Chem. Soc.*, 1999, **121**, 9599–9610.

34 D. Leitner, F. R. Neururer and S. Hohloch, Synthesis and electrochemical properties of molybdenum nitrido complexes supported by redox-active NHC and MIC ligands, *Dalton Trans.*, 2025, **54**, 582–594.

35 A. Coffinet, D. Specklin, Q. Le Dé, S. Bennaamane, L. Muñoz, L. Vendier, E. Clot, N. Mézailles and A. Simonneau, Assessing Combinations of $B(C_6F_5)_3$ and N_2 –Derived Molybdenum Nitrido Complexes for Heterolytic Bond Activation, *Chem. – Eur. J.*, 2023, **29**, e202203774.

36 D. V. Yandulov, R. R. Schrock, A. L. Rheingold, C. Ceccarelli and W. M. Davis, Synthesis and Reactions of Molybdenum Triamidoamine Complexes Containing Hexaisopropylterphenyl Substituents, *Inorg. Chem.*, 2003, **42**, 796–813.

37 M. R. Buchmeiser, D. Wang, R. Schowner, L. Stöhr, F. Ziegler, S. Sen and W. Frey, Synthetic and Structural Peculiarities of Neutral and Cationic Molybdenum Imido and Tungsten Oxo Alkylidene Complexes Bearing Weakly Coordinating N-Heterocyclic Carbenes, *Eur. J. Inorg. Chem.*, 2024, **27**, e202400082.

38 A. Eizawa, K. Arashiba, H. Tanaka, S. Kuriyama, Y. Matsuo, K. Nakajima, K. Yoshizawa and Y. Nishibayashi, Remarkable catalytic activity of dinitrogen-bridged dimolybdenum complexes bearing NHC-based PCP-pincer ligands toward nitrogen fixation, *Nat. Commun.*, 2017, **8**, 14874.

39 L. Merakeb, S. Bennaamane, J. De Freitas, E. Clot, N. Mézailles and M. Robert, Molecular Electrochemical Reductive Splitting of Dinitrogen with a Molybdenum Complex, *Angew. Chem., Int. Ed.*, 2022, **61**, e202209899.

40 P. Basu, V. N. Nemykin and R. S. Sengar, Syntheses, Spectroscopy, and Redox Chemistry of Encapsulated Oxo–Mo(v) Centers: Implications for Pyranopterin-Containing Molybdoenzymes, *Inorg. Chem.*, 2003, **42**, 7489–7501.

41 N. L. Creevey, A. G. McEwan, G. R. Hanson and P. V. Bernhardt, Thermodynamic Characterization of the Redox Centers within Dimethylsulfide Dehydrogenase, *Biochemistry*, 2008, **47**, 3770–3776.

42 R. A. Lal, A. Kumar, J. Chakraborty and S. Bhaumik, Molybdenum(vi), (V) and (IV) complexes with chiral benzoin thiosemicarbazone, *Transition Met. Chem.*, 2001, **26**, 557–562.

43 N. G. Connelly and W. E. Geiger, Chemical Redox Agents for Organometallic Chemistry, *Chem. Rev.*, 1996, **96**, 877–910.

44 P. Sampson, T. E. Janini and L. Fader, in *Encyclopedia of Reagents for Organic Synthesis (EROS)*, John Wiley & Sons, Ltd, 2007, DOI: **10.1002/047084289X**.

45 J.-M. Savéant and C. Costentin, in *Elements of Molecular and Biomolecular Electrochemistry*, John Wiley & Sons Inc., 2019, pp. 81–181, DOI: **10.1002/9781119292364.ch2**.

46 R. D. Feltham, Electron spin resonance and optical spectra of chromium "sandwich" compounds, *J. Inorg. Nucl. Chem.*, 1961, **16**, 197–203.

47 (*a*) CCDC 2515875: Experimental Crystal Structure Determination, 2026, DOI: **10.5517/ccdc.csd.cc2qfz8f**; (*b*) CCDC 2515876: Experimental Crystal Structure Determination, 2026, DOI: **10.5517/ccdc.csd.cc2qfz9g**; (*c*) CCDC 2515877: Experimental Crystal Structure Determination, 2026, DOI: **10.5517/ccdc.csd.cc2qfzbh**; (*d*) CCDC 2515878: Experimental Crystal Structure Determination, 2026, DOI: **10.5517/ccdc.csd.cc2qfzcj**; (*e*) CCDC 2515879: Experimental Crystal Structure Determination, 2026, DOI: **10.5517/ccdc.csd.cc2qfzdk**.